EFFECT OF ROUGH SURFACES ON GUIDED WAVES IN PLATES

D. E. Chimenti and O. I. Lobkis†
†Center for NDE and
Department of Aerospace Engineering & Engineering Mechanics
Iowa State University
Ames IA 50011

INTRODUCTION

The interaction of ultrasound with rough surfaces is being actively investigated, from both a theoretical and experimental standpoint. The problem is important to several areas, including ocean acoustics [1,2] and dielectric waveguides, such as optical fibers. In either of these problems the fields can be assumed to be represented by a single scalar potential. The problem we address here has previously received very little attention, and concerns the propagation of guided elastic waves in a planar solid waveguide having randomly rough surfaces with compressional and shear potentials that are coupled at each interface. The rough surface is intended to model incipient corrosion in aluminum aircraft structure.

Most theoretical treatments of the acoustic rough-surface problem fall into two categories: mean field integral transform methods [2–4], and perturbation methods [5,6]. More specific types of roughness have also been studied, namely scattering at periodic surfaces [7,8]. Elements of wave scattering in layered rough elastic solids have been treated in [9] and [5], but with no consideration of guided waves. A convenient simplification of this problem would be an approximate result for scattering from a randomly rough fluid-solid interface expressed in terms of the smooth surface reflection coefficient and the roughness parameters. Such was introduced by Eckhart [10], in which the scattered field is taken to be composed of two components: a random, incoherent component, owing to the rough surface scattering, and a residual coherent component. This approach, termed the phase-screen approximation (PSA), ignores any amplitude effects of the scattering and instead considers all the influence to be felt in the signal phase. Strictly speaking, the PSA is valid only when the elastic wavelengths in the solid are much larger than the rms roughness height h, and when the fluid wavelength is much less than the roughness correlation length L. This expression has also been derived by Nagy and Adler [11] and has been discussed by

Review of Progress in Quantitative Nondestructive Evaluation, Vol 16
Edited by D.O. Thompson and D.E. Chimenti, Plenum Press, New York, 1997

Rose and Nagy [12] and Dacol [13]. Using the PSA, comparisons to experimental measurements of fluid-solid RS ultrasonic scattering, in both transmission and reflection, have shown excellent agreement [11,12].

We report experimental measurements and a theoretical calculation of the propagation and reradiation of guided elastic waves in a planar fluid-loaded solid waveguide having rough surfaces. We adapt the PSA to the approximate treatment of waves in rough waveguides, because of its simplicity compared to more general calculations. We begin with a description of the calculation and its predictions, followed by the experimental data compared to the theoretical model. We show that the dependence of RS-induced wave damping on rms roughness height h, on wave frequency, and on acoustic beam separation, is fairly accurately predicted by our model, which uses the PSA to characterize the interaction of individual guided mode partial waves at the plate surfaces. In addition, we have observed a strong dependence of the effective wave damping on mode selection, owing to the dynamic behavior of partial wave energy in the plate, as predicted by our RS dispersion relation.

In an elastic waveguide it is well known that the guided wave mode can be decomposed into propagating or evanescent compressional and shear partial waves. To illustrate the rough-surface influence on the dispersion relation we calculate the behavior using PSA to model the interaction of the partial waves with the rough surfaces and exploiting the simplicity of the transverse resonance method [14] to obtain an exact analytical result that naturally incorporates the partial wave reflection coefficients at the guiding surfaces. The transverse resonance conditions are

$$\begin{aligned} \pm A_p e^{-\imath\kappa_p d} &= A_p \widehat{\Gamma}_{pp} e^{\imath\kappa_p d} + A_s \widehat{\Gamma}_{sp} e^{\imath\kappa_s d} \\ \pm A_s e^{-\imath\kappa_s d} &= A_p \widehat{\Gamma}_{ps} e^{\imath\kappa_p d} + A_s \widehat{\Gamma}_{ss} e^{\imath\kappa_s d}, \end{aligned} \tag{1}$$

where the $A_{p,s}$ are the compressional p and shear s partial wave amplitudes, $\widehat{\Gamma}_{ps}$ is the traction-free reflection coefficient for an incident compressional and reflected shear wave from a rough surface, and $2d$ is the plate thickness. The $\pm$ refers to symmetric or antisymmetric plate oscillations. Other similar terms $\widehat{\Gamma}_{ps}$, $\widehat{\Gamma}_{sp}$, and $\widehat{\Gamma}_{ss}$ are the scattering coefficients for indicated combinations of incident and reflected waves for a rough surface.

The transverse (x_3 projection) wavevector components κ_p (compressional) and κ_s (shear) are given by $\sqrt{\omega^2/V_{p,s}^2 - \xi^2}$, respectively, where ω is the angular frequency, $V_{p,s}$ are the compressional and shear wavespeeds, and ξ is the wavenumber of the propagating guided wave. The reflection coefficients (for coherent energy) $\widehat{\Gamma}_{\alpha\beta}$ ($\alpha = \{p,s\}$, $\beta = \{p,s\}$) for a rough surface are given, according to the phase-screen approximation (PSA), by a product of the smooth surface coefficient $\Gamma_{\alpha\beta}$ and the PSA contribution,

$$\widehat{\Gamma}_{pp,ss} = \Gamma_{pp,ss} e^{-2h^2\kappa_{p,s}^2}, \qquad \widehat{\Gamma}_{ps,sp} = \Gamma_{ps,sp} e^{-h^2(\kappa_p+\kappa_s)^2/2}. \tag{2}$$

Let ϵ, δ, and λ be defined as the p and s exponential terms in the above equations,

$$\epsilon = e^{-2h^2\kappa_p^2}, \qquad \delta = e^{-2h^2\kappa_s^2}, \qquad \lambda = e^{-h^2(\kappa_p+\kappa_s)^2/2}. \tag{3}$$

Substituting these into Eq (1), and using relations among the $\Gamma_{\alpha\beta}$ [14], the resulting homogeneous system will have a nontrivial solution if

$$\begin{aligned} \epsilon\delta\Gamma_{pp}^2 e^{\imath(\kappa_p+\kappa_s)d} \pm \epsilon\Gamma_{pp} e^{\imath(\kappa_p-\kappa_s)d} \mp \delta\Gamma_{pp} e^{-\imath(\kappa_p-\kappa_s)d} \\ + \lambda^2(1-\Gamma_{pp}^2)\, e^{\imath(\kappa_p+\kappa_s)d} - e^{-\imath(\kappa_p+\kappa_s)d} = 0. \end{aligned} \tag{4}$$

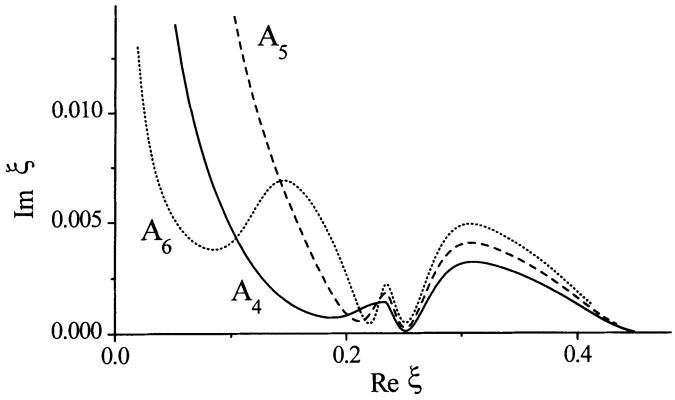

Figure 1: Pole trajectories in the complex plane for three antisymmetric plate modes, showing strong dependence of damping part on incident angle.

This is the dispersion relation for a rough surface waveguide, where we have used the PSA scattering model to account for sound damping effects of the rough guiding surfaces. This result can be further simplified so that it resembles a modified form of the smooth-surface Lamb wave dispersion equation.

Some representative solutions of Eq (4) are shown in Fig. 1 where the pole trajectories of three solutions of Eq (4) plotted as a parametric function of frequency. Examining the imaginary part of the guided wavenumber ξ, this component will vanish in a plate with smooth surfaces and in the absence of material losses. The large increase in imaginary ξ near each mode cutoff has a clearly intuitive explanation. As the mode approaches cutoff, the partial wavevectors are oriented nearly normal to the plate surface, implying many reflections per wavelength and leading to a large increase in surface-induced losses. At slightly higher frequency, for each mode, $\mathrm{Im}(\xi)$ falls to a low value, after which it increases and again decreases.

Close to the compressional critical angle branch point of the function in Eq (4), conversion of compressional to shear wave energy achieves a local maximum, compared to its value on either side of the critical wavevector. Further, RS damping is a competing effect which increases as ω^2. Farther along the pole trajectory, the p wave ceases to be a factor, and the s-wave damping increases. At higher frequency still, the s partial wavevector makes progressively larger angles with the plate normal, and the partial wave interaction with the RS decreases as the modes approach their real limiting value κ_s. This last aspect of the model, the vanishing of roughness-induced damping at large partial wave angles, is certainly not realistic since some damping clearly remains, even when the waves are evanescent, as in the case of Rayleigh waves [15]. However, for the Lamb wave problem we treat here, those partial waves near grazing incidence seldom intersect the surface and therefore make relatively small contributions to guided wave damping in our model. The fact that

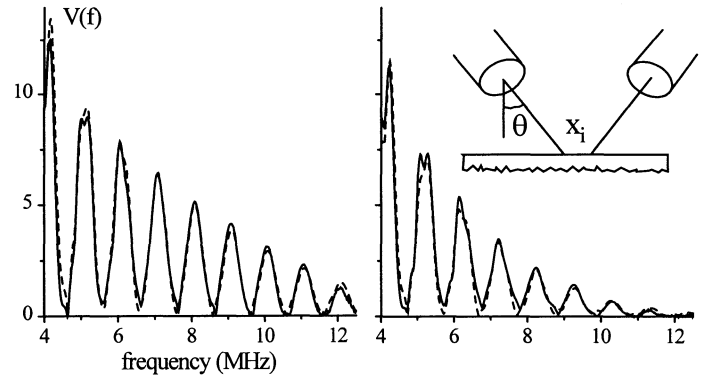

Figure 2: Experimental (solid) and theoretical (dashed) frequency dependence of the receiver voltage for smooth (left-hand frame) and rough (right-hand frame) surfaces (rms roughness $h = 26\,\mu$m), with x_i=20 mm, and incidence at 20°. Vertical scales are consistent between two plots. Inset shows experimental schematic.

the PSA may no longer be accurate for these rays has a much smaller effect on model accuracy. Moreover, operation near either critical wavespeed is not particularly useful for materials inspection with plate waves.

The inset of Fig. 2 shows a simplified schematic of the experimental geometry. The incident angle is θ and separation of the beam axes at the plate surface is x_i. In another work [16] we have calculated an exact 3-D voltage expression in a two-transducer geometry for an arbitrary reflection coefficient, which we use here to model the RS reflection measurements. In our experiments (see [16] for a description of the method) the samples have one rough and one smooth surface.

The voltage oscillations are the result of successive transverse resonances in the plate—interception by the incident beam of reflection coefficient zeroes as a function of frequency. The larger scale structure is caused by transducer diffraction and is well accounted for by our voltage model [16], including material damping [18]. In the top frame are the experimental data (solid) and theoretical prediction (dashed) of the frequency dependent voltage for a smooth plate (2.26-mm thick). Essentially all major features are accounted for.

To analyze these experimental data, a model different from the one expressed in Eq (4) is needed, one that can accommodate roughness on one plate surface only. We have accomplished this using the same partial-wave approach presented above, but applying it to an expression for the plate reflection coefficient written in terms of halfspace scattering relations [17]. The details of this calculation are straightforward, but lengthy. Briefly, the reflection expression is

$$R = R_h + \frac{T_p\left(\tau_{pf}\left(1-\tau_{ss}\right)+\tau_{sf}\tau_{ps}\right)+T_s\left(\tau_{sf}\left(1-\tau_{pp}\right)+\tau_{pf}\tau_{sp}\right)}{\left(1-\tau_{pp}\right)\left(1-\tau_{ss}\right)-\tau_{ps}\tau_{sp}} \tag{5}$$

where R_h is the halfspace reflection coefficient, and T_p and T_s are the joined halfspace

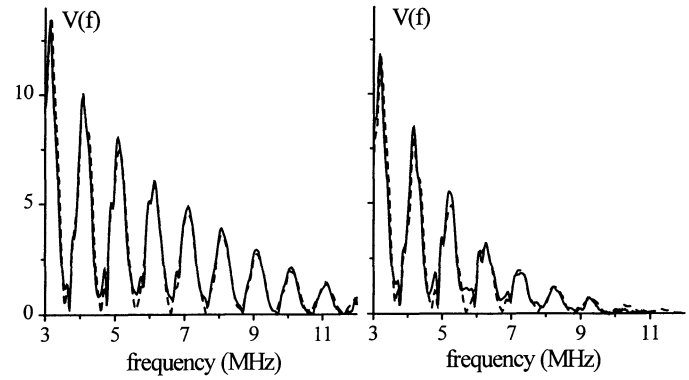

Figure 3: As Fig. 2 for the same samples, but with x_i=30 mm and incidence at 20°. Vertical scales are consistent between two plots. Good detailed agreement is seen with model calculation.

compressional and shear transmission coefficients for a fluid-solid interface. Also, R_h and $T_{p,s}$ are the rough-surface PSA equivalents to the smooth-surface counterparts. The term in Eq (5) $\tau_{\alpha\beta}$ is defined,

$$\tau_{\alpha\beta} = R^{II}_{\alpha p} R^{I}_{p\beta} + R^{I}_{\alpha s} R^{I}_{s\beta} \tag{6}$$

where f stands for fluid, and $R^{I,II}_{\alpha\beta}$ are reflection and transmission coefficients on solid-fluid interfaces I and II.

In Fig. 2 we plot the calculated and experimental smooth surface and rough surface reflected voltage spectra for a beam incident at an angle of 20° with $x_i = 20$ mm (as shown in the inset). The corresponding results for the 26-μm rms RS plate (2.22 mm thick), are recorded in the lower frame of Fig. 2, where the rough surface lies opposite the transducers. The vertical scales of the two sets of plots are internally consistent. Independent, high-frequency acoustic profilometry [12] performed on a larger sample from which the plate was fabricated, yields an rms roughness $h = 26$ μm. The two sets of curves, theory (dashed) and experiment (solid), show the same quantitative behavior, where we have assumed an rms roughness of 30 μm. There are no other adjustable parameters.

A second example of roughness-induced attenuation is shown in Fig. 3, where calculations and experimental data are presented for a smooth plate in the top frame and the same 26-μm RS in the bottom, but for a beam offset of $x_i = 30$ mm. The beam incident angle is 20°. The bottom frame shows the RS results, where we have used an estimate of 26 μm to model this data. The adjustment of the assumed roughness from 26 μm to 30 μm in the data of Fig. 2 might be accounted for by the fluctuation in the local rms roughness for these two measurements. Again, the vertical scales of Fig. 3(a) and (b) are consistent with each other, so that the signal decrease from roughness can be observed.

Contact measurements have also been performed. In Fig. 4 we show the results of

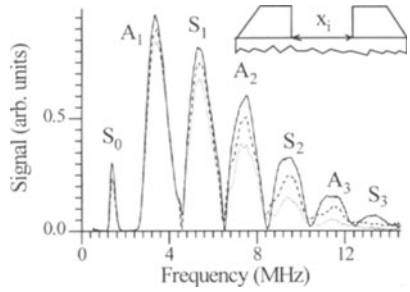

Figure 4: Shoe-contact experimental signal from rough aluminum plates ($h = 26$ μm) for three different transducer separations x_i (solid: 20 mm; dashed: 30 mm; dotted: 40 mm); inset shows geometry.

measurements on the same sample, but done with contact transducers at a plate phase velocity of 3.32 km/s, where extensive averaging is necessary to achieve reproducible results. Here, each peak corresponds to a mode (lebeled on the plot), and the successive curves solid for 20-mm transducer separation, dashed is 30 mm, and dotted is 40 mm. The inset shows the experimental arrangement. Then, in Fig. 5 are the collected data for three of the modes for this sample ($h = 26$ μm and $d = 2.22$ mm). The slopes of the lines represent the increas in damping. When these data are compared to those from the 13-μm sample, a slope ratio of 4.5 is found. The quadratic rms roughness dependence suggests a ratio of 4.

Finally, the experimental data from two knife-edge transducers ($x_i = 22$ mm) is shown in Fig. 6, where the three curves correspond to smooth (solid), 13-μm roughness (dashed), and 26-μm roughness (dotted). There are several interesting effects here. First, the smooth-surface curve shows a rapid drop in amplitude after 6 MHz. The transducer bandwidth alone cannot account for this effect. The amplitude also depends on the spectrum of energy in the plate and its leakage rate out of/into the knife-edge (tip width ≈ 1 mm). The 13-μm surface shows a higher loss version of this same behavior, while the curve dips dramatically for the 26-μm surface (dotted). The influence of h^2 on these curves is quite apparent. And, the effects are complicated by the fact that at low frequency, the knife-edge is nearly a line source, while at 10 MHz, it is broadcasting energy into a narrow cone of angles about 12° wide.

SUMMARY

While not perfect, particularly near critical angles, the generally good agreement between model and experiment suggests the soundness of our modeling approach in the range where practical roughness measurements would likely be made and demonstrates that a simple, yet accurate, model of rough surface elastic waveguide propagation is indeed possible.

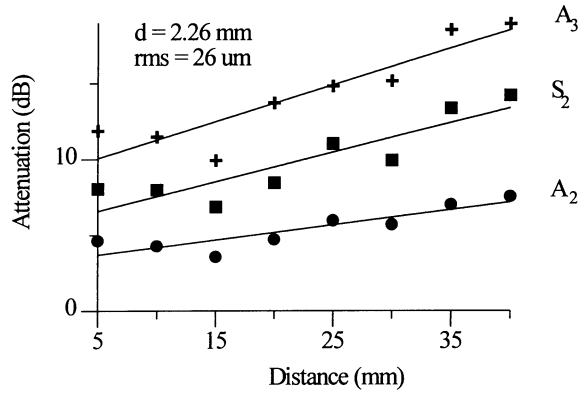

Figure 5: Collected experimental data for rough aluminum plates as a function of transducer separations x_i; three modes are illustrated for $h = 26$ μm.

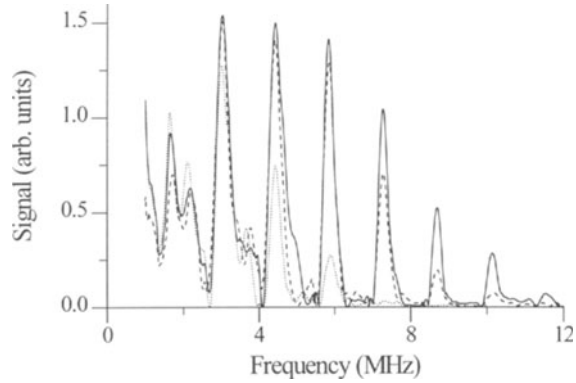

Figure 6: Knife-edge contact experimental signals from rough aluminum plates (dashed: $h = 13$ μm; dotted: $h = 26$ μm) for a transducer separation $x_i = 22$ mm. Sharp decrease in received signal from 26-μm RS between 3 and 8 MHz illustrates effect of narrowing spatial bandwidth.

ACKNOWLEDGEMENTS

Support from AFOSR Grant F49620-95-1-0294 is gratefully acknowledged. We thank M. Rudolph for valuable programming assistance.

REFERENCES

1. J. A. Ogilvy, *Theory of Wave Scattering from Random Rough Surfaces*, (Adam Hilger, Bristol, 1991).
2. F. G. Bass and I. M. Fuks, *Wave Scattering from Statistically Rough Surfaces*, (Pergamon Press, Oxford, 1979).
3. D. K. Dacol and D. H. Berman, J. Acoust. Soc. Am. 84, 292-302 (1988).
4. D. H. Berman, J. Acoust. Soc. Am. 96, 417-26 (1994).
5. W. A. Kuperman and H. Schmidt, J. Acoust. Soc. Am. 86, 1511-22 (1989).
6. H. Schmidt and W. A. Kuperman, J. Acoust. Soc. Am. 97, 2199-209 (1995).
7. A. Lakhtakia, V. K. Varadan, and V. V. Varadan, J. Appl. Phys. 60, 4090-4 (1986).
8. A. El-Bahrawy, J. Acoust. Soc. Am. 96, 3155-66 (1994).
9. J. D. Sheard and M. Spivak, J. Acoust. Soc. Am. 97, 72-83 (1995).
10. C. Eckhart, J. Acoust. Soc. Am. 25, 556 (1953).
11. P. B. Nagy and L. Adler, J. Acoust. Soc. Am. 82, 193-7 (1987).
12. J. H. Rose and P. B. Nagy, J. Appl. Phys. 73, 566-80 (1993).
13. D. K. Dacol, J. Acoust. Soc. Am. 88, 978-83 (1990).
14. B. A. Auld, *Acoustic Waves and Fields in Solids*, 2nd ed, (Krieger, Malabar, FL, 1990).
15. E. I. Urazakiv and L. A. Falkovskii, Sov. Phys. JETP 36, 1214–16 (1973).
16. O. I. Lobkis, A. Safaeinili, and D. E. Chimenti, J. Acoust. Soc. Am. 99, 2727-36 (1996).
17. M. Deschamps and C.-W. Cao, Ultrasonics 29, 288-93 (1991).
18. W. P. Mason and H. J. McSkimin, J. Acoust. Soc. Am. 19, 464-73 (1947).